

# Computational study for the effects of coil configuration on blood flow characteristics in coil-embolized cerebral aneurysm

Tomohiro Otani<sup>1</sup> · Satoshi Ii<sup>1</sup> · Tomoyoshi Shigematsu<sup>2</sup> · Toshiyuki Fujinaka<sup>2</sup> · Masayuki Hirata<sup>2</sup> · Tomohiko Ozaki<sup>2</sup> · Shigeo Wada<sup>1</sup>

Received: 6 October 2015 / Accepted: 29 June 2016 / Published online: 21 July 2016  
© International Federation for Medical and Biological Engineering 2016

**Abstract** Coil embolization of cerebral aneurysms with inhomogeneous coil distribution leads to an incomplete occlusion of the aneurysm. However, the effects of this factor on the blood flow characteristics are still not fully understood. This study investigates the effects of coil configuration on the blood flow characteristics in a coil-embolized aneurysm using computational fluid dynamics (CFD) simulation. The blood flow analysis in the aneurysm with coil embolization was performed using a coil deployment (CD) model, in which the coil configuration was constructed using a physics-based simulation of the CD. In the CFD results, total flow momentum and kinetic energy in the aneurysm gradually decayed with increasing coil packing density (PD), regardless of the coil configuration attributed to deployment conditions. However, the total shear rate in the aneurysm was relatively high and the strength of the local shear flow varied based on the differences in coil configuration, even at adequate PDs used in clinical practice (20–25 %). Because the sufficient shear rate reduction is a well-known factor in the blood clot formation occluding the aneurysm inside, the present study gives useful insight into the effects of coil configuration on the treatment efficiency of coil embolization.

**Keywords** Cerebral aneurysm · Computational fluid dynamics · Coil embolization

✉ Shigeo Wada  
shigeo@me.es.osaka-u.ac.jp

<sup>1</sup> Department of Mechanical Science and Bioengineering, Graduate School of Engineering Science, Osaka University, Machikaneyama-cho 1-3, Toyonaka, Osaka 560-8531, Japan

<sup>2</sup> Department of Neurosurgery, Graduate School of Medicine, Osaka University, 2-2 Yamadaoka, Suita, Osaka 560-0871, Japan

## 1 Introduction

Coil embolization is a popular clinical method used to treat cerebral aneurysms. In this procedure, several coils are deployed in the aneurysm to stagnate blood flow and enhance blood clot formation, occluding the aneurysm inside. A high packing density (PD) of the coils in the aneurysm (>20–25 %) is generally desirable to maintain long-term stability [31, 32], and this amount has been widely used for an evaluation index in clinical practice. However, recent clinical statistics have shown that the degree of PD cannot be the only factor in predicting stability for any clinical case [28, 29]; instead, the spatial distribution or configuration of the coils, especially in the neck region, has gradually become a mainstream index [13, 29, 35, 36] in terms of the prevention of the aneurysm inflow [7]. Because the incomplete prevention of the inflow induces the risk of aneurysm recurrence, a detailed evaluation of the effects of the coil configuration on the blood flow characteristics in the aneurysm is required to increase the treatment effectiveness of coil embolization.

Computational fluid dynamics (CFD) is an effective tool used to reveal the detailed characteristics of the blood flow in the coil-embolized aneurysm, and various kinds of CFD studies have been attempted [1, 3, 5, 6, 12, 15–17, 20–23, 25–27, 30]. In clinical practice, several coils are manually deployed in the aneurysm using a microcatheter, and a complex structure is constructed. To avoid having to deal with such geometric complexity in the CFD studies, simplified approaches using the porous media (PM) model have been developed, in which the blood flow in the coil-embolized aneurysm is assumed to be a flow in a homogeneous porous medium [6, 16, 17, 20, 25]. The blood flow analyses using the PM model give an understanding

of the effects of PD on global flow stagnation; however, the PM model has a critical limitation when analyzing the local flow characteristics in the coil-embolized aneurysm because of the implicit expression of the presence of the coil.

To address this issue, several CFD approaches using realistic coil configurations have been proposed [1, 5, 15, 21–23, 26, 27, 30]. Morales et al. [21, 22] proposed a rule-based technique to represent a realistic coil configuration called dynamic path planning, in which the path of the coil is generated using a potential field based on a geometric constraint. According to CFD studies using their model, variations of the spatiotemporally averaged velocities in the aneurysm gradually decreased with increasing PD [21]. Also, Babiker et al. [1] analyzed the blood flow in the aneurysm based on coil deployment, where the coils were deployed using a solid deformation analysis comprising beam elements. In the CFD studies, they investigated the effects of the PD, the neck size of the aneurysm and the flow in the parent artery, on the reduction of the inflow and spatial-averaged velocity in the coil-embolized aneurysm. These existing CFD studies using realistic coil configurations essentially focused on the overall flow stagnation rather than the local flow characteristics. Otani et al. [26, 27] focused on the local flow characteristics in the aneurysms following coil deployment and found it was highly disturbed around the coils, especially in the neck region of the aneurysm. This suggests that a difference in coil configuration also gives rise to a difference in local flow characteristics, i.e., local stagnation and shear flow reduction, which is believed to play an important role in sustaining long-term stability [13, 29, 35, 36] and be a key component in the process of blood clot formation [4, 10, 32, 36], occluding the aneurysm inside. Therefore, a reliable CFD simulation that aims to reveal the effects of the coil configuration on the local flow field is necessary to fully understand the treatment effectiveness of coil embolization.

In the present study, we investigate the effects of the coil configuration on the blood flow characteristics through a case study analysis of the CFD simulation using patient-specific geometry of the cerebral aneurysm. Various flow fields in the aneurysm with various coil configurations are obtained using the coil deployment (CD) model, in which the coil deployment is obtained through a physics-based simulation that takes account of force-balances between stretching, bending and repulsive forces between the coil–aneurysm and coil–coil contacts [26]. To clarify the effects of the coil configuration more vividly, a flow analysis with the PM model [25] is also carried out, and the results are compared in both models. Through the comparison, we also discuss the utility and limitations of the PM model.

## 2 Methods

### 2.1 Construction of the patient-specific aneurysm model

A patient-specific geometry of the cerebral aneurysm was acquired from clinical CT images in Osaka University hospital. The aneurysm was formed in the internal carotid artery, and its longest diameter was approximately 7 mm. The clinical CT image stack consisted of 145 slices of  $512 \times 512$  pixels, where the pixel size was 0.1875 mm and voxel depth was 0.625 mm.

The three-dimensional (3-D) reconstruction of the aneurysm geometry was done using the Amira 5.4.2 (Visage Imaging, Berlin, Germany). The aneurysm surface was given by 3-D triangle meshes based on the unconstrained smoothing function of Amira (Fig. 1a). To reduce the remaining spatial irregularity in the obtained surface meshes, a physics-based surface smoothing process was carried out (Fig. 1b), in which the stretching and bending resistance were applied to each edge of the mesh and pair of the adjacent meshes, respectively. We evaluated the volume and surface area of the whole aneurysm geometries between the aneurysm geometries prior to and after smoothing processing. We confirmed that both changes were less than 2 %, and thus concluded that the smoothing processing satisfactorily preserved the characteristics of the original surfaces.

### 2.2 Coil deployment simulation

The coil deployment simulation was implemented based on the physics-based approach [26]. In the coil deployment simulation, the coil was constructed by assuming that it was an elastic wire with stretching and bending resistances (Fig. 2a). The coil was discretized by a set of line elements with an initial length  $L_0$ , and linear springs with a spring constant  $k_s$  for stretching, and  $k_b$  for bending. We assign the index of each element and node with  $j$  ( $j = 1, 2, \dots, M$ ) and  $i$  ( $i = 1, 2, \dots, N$ ), where  $M$  and  $N$  indicate the total number of elements and nodes, respectively.

The elastic energy for stretching of the coil,  $W_s$ , is defined by

$$W_s = \frac{1}{2} k_s \sum_{j=1}^M (l_j - l_0)^2, \quad (1)$$

where  $l_j$  is the current length of the line element. In the same manner, the elastic energy for bending the coil,  $W_b$ , is defined by

$$W_b = \frac{1}{2} k_b \sum_{i=1}^N (\theta_i - \theta_0)^2, \quad (2)$$

**Fig. 1** Process of the construction of the aneurysm geometry from clinical CT images. The patient-specific geometry of the aneurysm is extracted from a medical CT image and surface meshes are constructed (a). The surface smoothing is done by a physics-based surface smoothing process (b). The inlet and outlet regions are set, and volumetric meshes are constructed for flow analyses (c). The aneurysm region in green is defined for the coil deployment simulation of the CD model and flow analyses with the PM model (d)

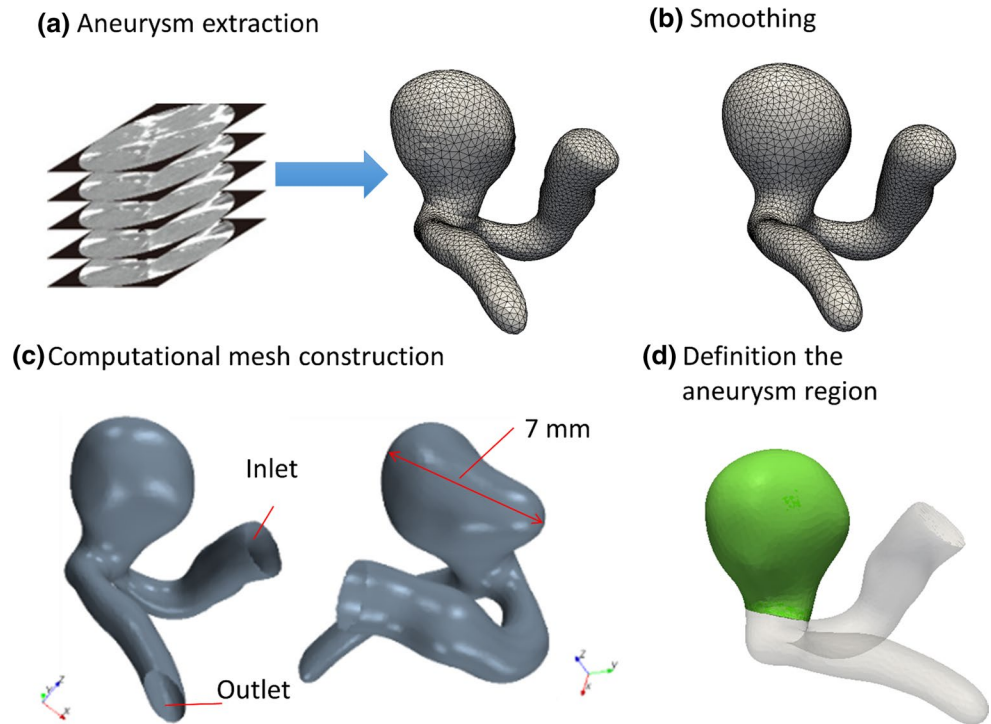
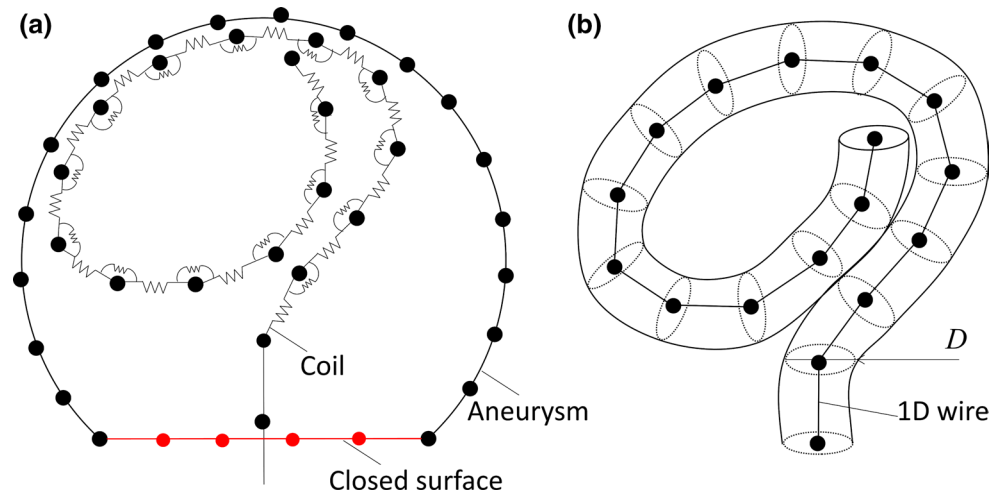


**Fig. 2** Schematic drawing of the coil deployment simulation (a) and the volumetric coil configuration (b)



where  $\theta_0$  and  $\theta_i$  are the angles between neighboring line elements at the reference and current states, respectively. Here, we assume a straight coil at the reference state, i.e.,  $\theta_0 = \pi$ .

The total elastic energy of the coil is given by

$$W = W_s + W_b. \tag{3}$$

According to the virtual work theory, the elastic force at the node  $i$ ,  $\mathbf{F}_i$ , is written by

$$\mathbf{F}_i = -\frac{\partial W}{\partial \mathbf{x}_i}, \tag{4}$$

where  $\mathbf{x}_i$  is the position vector of node  $i$ .

The mechanical interactions from a coil–aneurysm contact and coil–coil contact are modeled by the linear spring-dashpot model, which is widely employed in discrete element methods, e.g., [19]. In the contact between node  $i$  of the coil with position vector  $\mathbf{x}_i$  and an arbitrary node constituting the triangle mesh of the aneurysm surface with position vector  $\mathbf{x}_a$ , the repulsive force  $\mathbf{F}_{a,i}$  is described by

$$\mathbf{F}_{a,i} = \begin{cases} k_{\text{con}}(\mathbf{x}_i - \mathbf{x}_a) + \eta_{\text{con}}\dot{\mathbf{x}}_i & |\mathbf{x}_i - \mathbf{x}_a| < \frac{D}{2}, \\ \mathbf{0} & \text{otherwise} \end{cases}, \tag{5}$$

where  $k_{\text{con}}$  is the spring constant,  $D$  is the diameter of the coil, the dot over  $\mathbf{x}$  means the material derivative and  $\eta_{\text{con}}$  is the dumping coefficient derived from the energy loss upon collision [19] such that

$$\eta_{\text{con}} = -2 \ln e_{\text{con}} \sqrt{\frac{m_{\text{con}} k_{\text{con}}}{\pi^2 + (\ln e_{\text{con}})^2}}, \quad (6)$$

where  $e_{\text{con}}$  is the coefficient of restitution and  $m_{\text{con}}$  is the mass given by

$$m_{\text{con}} = \frac{m_1 m_2}{m_1 + m_2}, \quad (7)$$

where  $m_1$  and  $m_2$  are the masses assigned at two contact nodes. Equation (5) indicates that a repulsive force is generated when the distance between the coil and the wall is lower than the radius of the coil. Here, the aneurysm wall is assumed to be rigid; i.e., the surface meshes of the aneurysm are fixed even if an interaction force is exerted on the surface from the coils. In this case, the mass of nodes in the aneurysm surface is assumed to be negligibly large, and thus the  $m_{\text{con}}$  can be expressed as the mass  $m$  assigned at each node of the coil.

We insert several coils in a step-by-step manner and deploy them. Thus, we address self–self and self–other coil interactions. Now, we introduce the repulsive force  $\mathbf{F}_{c,i}$  exerted on node  $i$  as

$$\mathbf{F}_{c,i} = \begin{cases} k_{\text{con}}(\mathbf{x}_i - \mathbf{x}_k) + \eta_{\text{con}}(\dot{\mathbf{x}}_i - \dot{\mathbf{x}}_k) & |\mathbf{x}_i - \mathbf{x}_k| < D \\ \mathbf{0} & \text{otherwise} \end{cases}, \quad (8)$$

$$\mathbf{F}_{c,k} = -\mathbf{F}_{c,i}, \quad (9)$$

where  $\mathbf{x}_k$  is the position vector of another node ( $i \neq k$ ) in the inserted and already deployed coils.  $\mathbf{F}_{c,k}$  is the counterpart of the interaction forces attributed to the principle of action and reaction, and thus induces the motion of already deployed coils. Here, the mass assigned at the node was set to be same ( $m = m_1 = m_2$ ), so  $m_{\text{con}}$  can be calculated to be  $m/2$ .

With the forces defined in Eqs. (4), (5), (8) and (9), the equation of motion for node  $i$  is described by

$$m\ddot{\mathbf{x}}_i + \nu\dot{\mathbf{x}}_i = \mathbf{F}_i + \mathbf{F}_{a,i} + \mathbf{F}_{c,i} + \mathbf{F}_0, \quad (10)$$

where  $\nu$  is the damping coefficient and  $\mathbf{F}_0$  is the external force used to insert the coil into the aneurysm. The coil deployment simulation is done by solving Eq. (10) in a step-by-step manner. Using a semi-implicit Euler scheme, the discrete form of Eq. (10) is given by

$$m \frac{^{t+1}\dot{\mathbf{x}}_i - {}^t\dot{\mathbf{x}}_i}{\Delta t} + \nu {}^t\dot{\mathbf{x}}_i = {}^t\mathbf{F}_i + {}^t\mathbf{F}_{a,i} + {}^t\mathbf{F}_{c,i} + {}^t\mathbf{F}_0, \quad (11)$$

$$\frac{^{t+1}\mathbf{x}_i - {}^t\mathbf{x}_i}{\Delta t} = {}^{t+1}\dot{\mathbf{x}}_i, \quad (12)$$

**Table 1** Parameters used in the coil deployment simulation

Spring constant (stretching)	$k_s$ (N/m)	$1.0 \times 10^5$
Spring constant (bending)	$k_b$ (N/rad)	$1.0 \times 10^{-3}$
Spring constant (contact)	$k_{\text{con}}$ (N/m)	$1.0 \times 10^5$
Coefficient of restitution (contact)	$e_{\text{con}}$ (–)	0.1
Mass assigned at the node	$m$ (kg)	$1.84 \times 10^{-7}$
Damping coefficient	$\nu$ (kg/s)	$1.0 \times 10^{-3}$
External force	$ \mathbf{F}_0 $ (N)	$1.8 \times 10^{-6}$
Coil diameter	$D$ (mm)	$2.54 \times 10^{-1}$
Total initial coil length	$L$ (mm)	$3 \times 10^2$
Initial element length	$l_0$ ( $\mu\text{m}$ )	$2.54 \times 10^{-1}$
Time increment	$\Delta t$ (s)	$8.5 \times 10^{-8}$

where  $\Delta t$  is the time increment. Velocity and position vectors are solved by iterating Eqs. (11) and (12), respectively.

The parameters used for the deployment simulation are shown in Table 1. The shape of the practically used coil is a single helix consisting of a platinum wire. Thus, the tensional resistance of the coil is composed mainly of the longitudinal and torsional resistances of the platinum wire, which makes it difficult to determine the tensional properties of the coil itself. Thus, in this study, the physical parameters are empirically determined to perform the realistic behavior of the coil. The initial total length of the coil  $L$  and the diameter of the coil  $D$  are determined from the information of a practically used coil [38]. The number of nodes (or elements) is determined such that the initial element size of a coil  $l_0$  is around the coil diameter  $D$ .

To avoid moving the coil out of the aneurysm in the process of coil deployment, a closed surface consisting of the triangle meshes is constructed between the aneurysm region (Fig. 1d) and arterial region. The initial coil configuration is set to be straight, and the head of the coil is located at the arbitrary place in the aneurysm region. To drive coil motion, the external force  $\mathbf{F}_0$  is imposed at the nodes outside of the aneurysm in the axial direction until all the nodes on the coil are entered into the aneurysm region. Then, a steady-state solution is obtained after the coil motion is negligibly small; i.e., the force balance of the right-hand side term in Eq. (10) is enough to satisfy a discretization level.

Once the 3-D distribution of the one-dimensional (1-D) coil is obtained from the deployment simulation, the volumetric coil configuration for the blood flow analysis is constructed by taking the coil diameter/length, as the central axis of the coil configuration is assigned to the distribution of the 1-D coil obtained in the coil deployment simulation (see Fig. 2b). Here, we neglect a change of coil diameter/length along the axial extension based on Poisson's effect, because the axial extension might be small in practical situations and its contribution to the diameter change is also



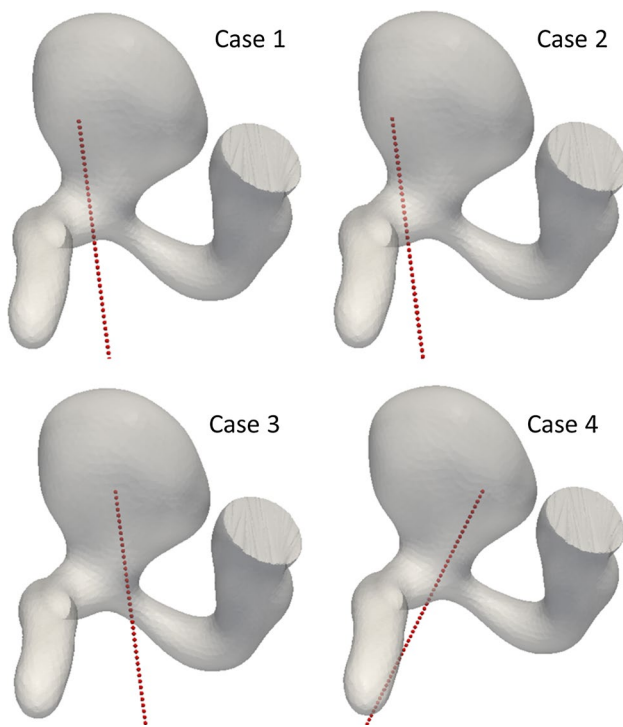


**Fig. 3** Four cases of coil deployment simulation by changing the deployment orientation and position. Red circles show the nodes of the coil

small. Thus, in this study, the coil is uniformly expanded with the given coil diameter  $D$ . Triangle meshes are used to represent the coil surface geometry.

The coil PD is calculated by the same methodology in clinical practice, given by

$$PD[\%] = 100 \frac{\pi n D^2 L}{4V}, \tag{13}$$

where  $n$  is the number of coils and  $V$  is the volume of the aneurysm. Three coils were deployed in total, with PDs of approximately 9, 18 and 27 %, respectively. To investigate the effects of coil configuration on blood flow, four cases of coil deployment simulation were conducted by changing the deployment orientation and position (Fig. 3).

### 2.3 Mesh construction

Volumetric meshes for fluid analyses were generated using the commercial software STAR-CCM + 6.04.014 (CD-Adapco, Yokohama, Japan) (Fig. 1c). Both the surface triangular meshes of coils and the aneurysm constructed in Sect. 2.2 were used for the mesh construction. Polyhedral meshes with five prism layers near the wall were used, in which the mesh parameters were determined such that the base size of the mesh was approximately 0.25 mm (minimum proximity was 10 % of the base size) and the

thickness of the prism layer was approximately 20 % of the base size. The numbers of volumetric meshes in the PD of 0, 9, 18 and 27 % were approximately 600,000, 2,400,000, 3,500,000, and 7,200,000, respectively. It should be noted that we checked mesh size dependency on the solutions through comparison with a solution using a finer base size of 0.2 mm and found that the differences in the solutions we will discuss were quite small, lower than 3 %. Thus, we determined that the ideal mesh size is approximately 0.25 mm, from the viewpoint of computational cost.

### 2.4 Blood flow analysis

#### 2.4.1 Governing equations and calculation conditions

We assume that the blood is an incompressible Newtonian fluid, because the non-Newtonian features were reported to be insufficient to alter the main flow pattern in the coil-embolized aneurysm [23]. Our preliminary analyses also showed that the non-Newtonian features were secondary for the solution we will discuss (data not shown). Although blood flow should be basically treated as a pulsatile flow, flow is assumed to be steady, because this assumption is a reasonable approximation to allow us to understand the temporally averaged flow characteristics in a cardiac cycle for blood flow analysis in cerebral aneurysms [14]. The steady incompressible Navier–Stokes equations are given by

$$\rho(\mathbf{u} \cdot \nabla \mathbf{u}) = -\nabla p + \mu \nabla^2 \mathbf{u}, \tag{14}$$

$$\nabla \cdot \mathbf{u} = 0, \tag{15}$$

where  $\mathbf{u}$  is the velocity vector,  $\rho$  is the pressure,  $\rho$  is the density, and  $\mu$  is the viscosity. In this study,  $\rho = 1.05 \times 10^3 \text{ kg/m}^3$  and  $\mu = 3.5 \times 10^{-3} \text{ Pa s}$  are used. The Eqs. (14) and (15) were solved with coupling using the SIMPLE algorithm, and its convective term was treated by the second-order upwind scheme.

We impose the following conditions on the boundaries of the artery and aneurysm (Fig. 1c): a uniform velocity at the inlet; zero pressure and zero velocity gradient at the outlet; no-slip condition at the fixed walls of the artery and aneurysm. The Reynolds number at the entrance of the inlet is approximately 230 [2]. The equations are solved by the SIMPLE algorithm with the finite volume method using STAR-CCM + 6.04.014.

#### 2.4.2 Blood flow analysis with PM model

Blood flow analyses with the PM model used in [25] were also performed to compare the results. In this analysis, we imposed the PM model only on the aneurysm region (Fig. 1d), where the flow was modeled as a flow in

a homogeneous porous medium that obeys Darcy's law. The pressure is modeled as locally balanced in these flow regions with resistance forces such that

$$0 = -\nabla p - K\mathbf{u}, \quad (16)$$

where  $K$  is the permeability of the porous medium. The permeability  $K$  is assumed to be a quasi-linear function of a flow velocity magnitude such that

$$K = \alpha|\mathbf{u}| + \beta, \quad (17)$$

where  $\alpha$  and  $\beta$  are coefficients. According to the Ergun equation [9] that describes the pressure drop in flow through homogeneous PM with spherical pores, the coefficient values of  $\alpha$  and  $\beta$  are given by

$$\alpha = \frac{1.75\rho(1-\kappa)}{\kappa^3 D_p}, \quad (18)$$

$$\beta = \frac{150\mu(1-\kappa)^2}{\kappa^3 D_p^2}, \quad (19)$$

where  $\kappa$  ( $0 \leq \kappa \leq 1$ ) is the porosity of the PM, and  $D_p$  is the diameter of the spherical pores, which is set to the coil diameter  $D$ . The PD is given by  $PD = 100(1-\kappa)$  using the porosity  $\kappa$ . In this study, the PD is set from 10 to 30 % in increments of 5 %.

### 3 Results

#### 3.1 Coil configuration

Typical solutions for the coil configurations with PDs of 9, 18 and 27 % are shown in Fig. 4a–c, respectively. The coils fill in the aneurysm from the surface to center with increasing PD. The coil was initially placed around the surface of the aneurysm, and thus a large space remained in the

center region at a low PD of 9 %. An additional coil was deployed, with the existing (initially inserted) coil at a PD of 18 %. The final coil deployed in the aneurysm filled the center region and pushed the other coils aside. As a result, the coils filled the entirety of the aneurysm.

To measure the distribution of the coils quantitatively, the coils were implicitly defined as a discrete indicator function on 3-D Cartesian meshes, using the method of [34]. Here, we used a mesh resolution of 0.05 mm. The center of the Cartesian meshes corresponds to the gravity point of the aneurysm. The local PD in the range of the radial thickness  $\Delta r$  of 0.25 mm is calculated by

$$\text{local PD}_m[\%] = 100 \frac{\sum_g \varphi_c(\mathbf{x}_g)}{\sum_g \varphi_a(\mathbf{x}_g)}, \quad \text{for } |\mathbf{x}_g| \in [m\Delta r, (m+1)\Delta r], \quad (20)$$

( $m = 1, 2, \dots$ ), where  $\mathbf{x}_g$  is the central point of the mesh and  $\varphi_c$  and  $\varphi_a$  are the indicator functions of the coil and aneurysm, respectively.

Figure 5 shows the radial distribution of the coils from the aneurysm center with respect to each PD. At a low PD of 9 %, the averaged local PD was lower than 3 % with a radius from 0 mm to 2 mm, whereas it stayed at approximately 10 % with a radius from 3 mm to 4 mm. It became approximately 0 % for  $r > 4.25$  mm. This inhomogeneity grew gradually milder with increasing PD. However, the variation of PD caused by differences in the deployment conditions remained, particularly in the center region of the aneurysm ( $r < 1$  mm), even at a high PD of 27 %.

#### 3.2 Blood flow analysis

Flow characteristics in the coil-embolized aneurysm were investigated using flow analyses with both the CD model and the PM model. Figure 6 shows the magnitude of the flow velocity in the cross-sectional plane of the aneurysm.

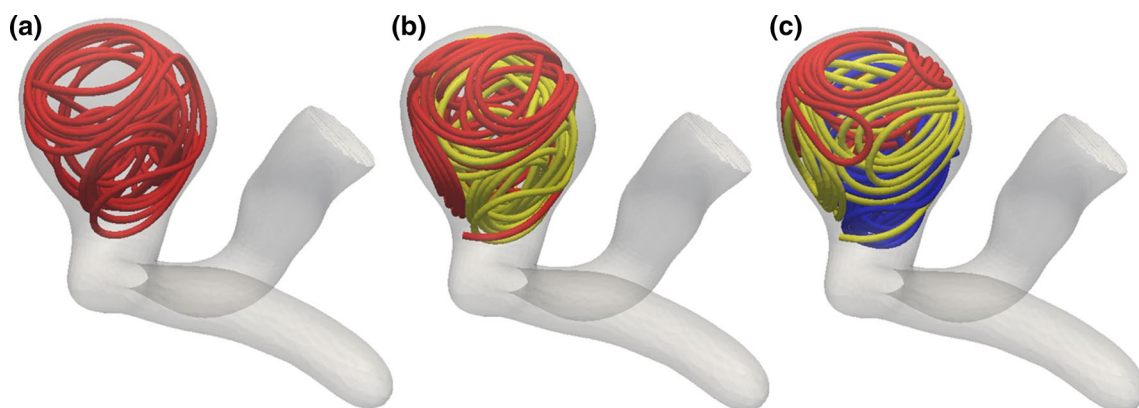


**Fig. 4** Configuration of the coils in the aneurysm at a packing density of 9 % (a), 18 % (b) and 27 % (c) in case 1

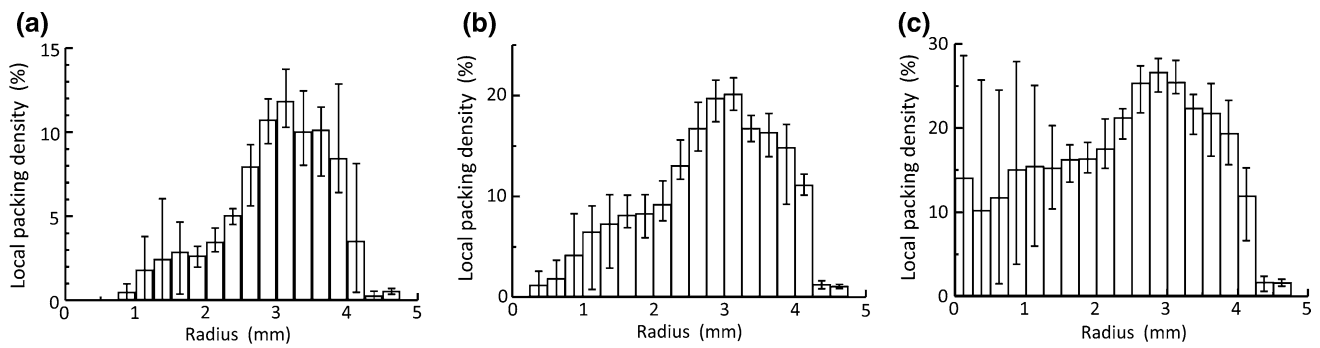


**Fig. 5** Local packing density in a volume with a radial thickness  $\Delta r = 2.5 \times 10^{-4}$  m at a packing density of 9 % (a), 18 % (b), and 27 % (c). Error bars show the maximum and minimum values of the results of the coil deployment simulation ( $n = 4$ )

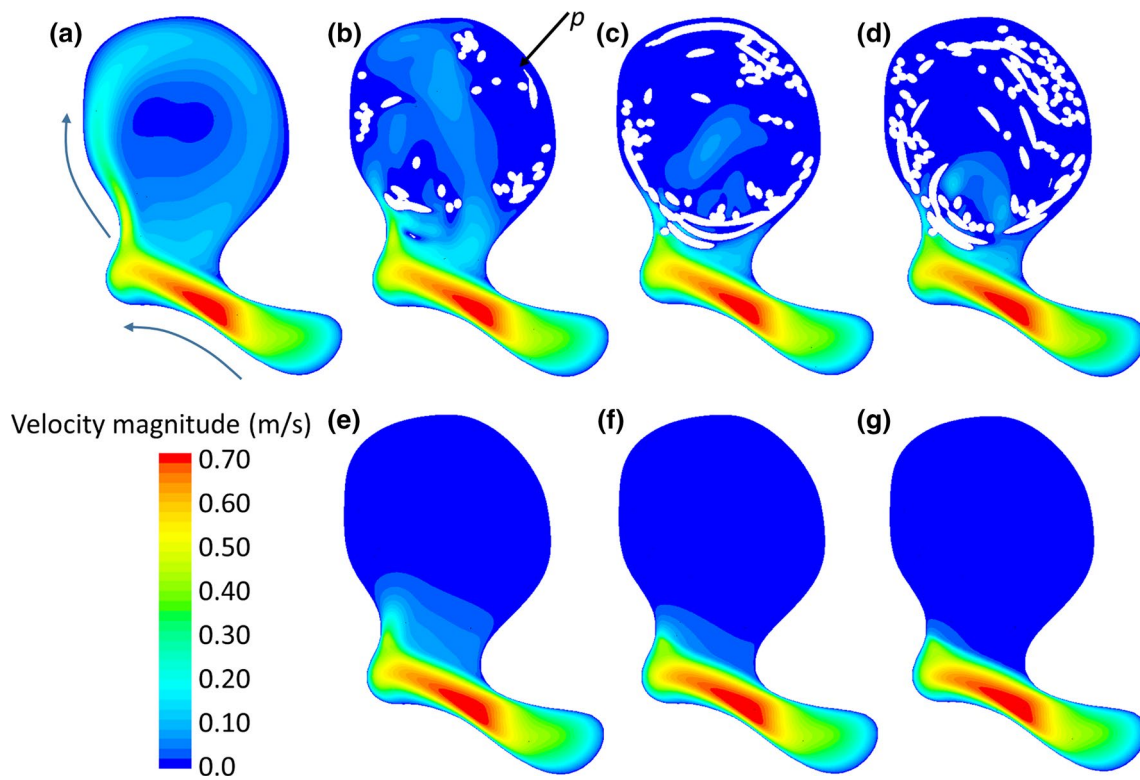


**Fig. 6** Magnitude of blood flow velocity in the cross-sectional plane of the aneurysm before coil embolization (a). Blue arrows show the flow direction. The results of the CD model at the packing densities of 9, 18 and 27 % are illustrated in b–d, respectively. The arrow *p*

shows the inner region of the aneurysm. The bottom panels show the results of the PM model at packing density 10 % (e), 20 % (f) and 30 % (g)

Prior to the coil embolization, the flow entered the distal neck region of the aneurysm, swirled around the aneurysm wall with decreasing velocity magnitude, and finally flowed out of the aneurysm into the proximal neck region (Fig. 6a). In the results of the CD model (Fig. 6b–d), the flow entered through a space in the existing coils, and its velocity decreased in the inner region (shown by arrow *p* in Fig. 6b). The swirling flow found prior to the coil embolization vanished at the low PD of 9 %. The flow velocity globally

decreased with increasing PD, whereas a relatively high magnitude of flow velocity remained in the neck region of the aneurysm even at the high PD of 27 %. In the results of the PM model (Fig. 6e–g), the magnitude of the flow velocity globally decreased from the middle to the inner region of the aneurysm, even at PD = 10 %. Flow stagnation occurred throughout the whole aneurysm with the increase of PD.

A change of the shear flow field in the aneurysm was investigated by introducing the shear rate defined by

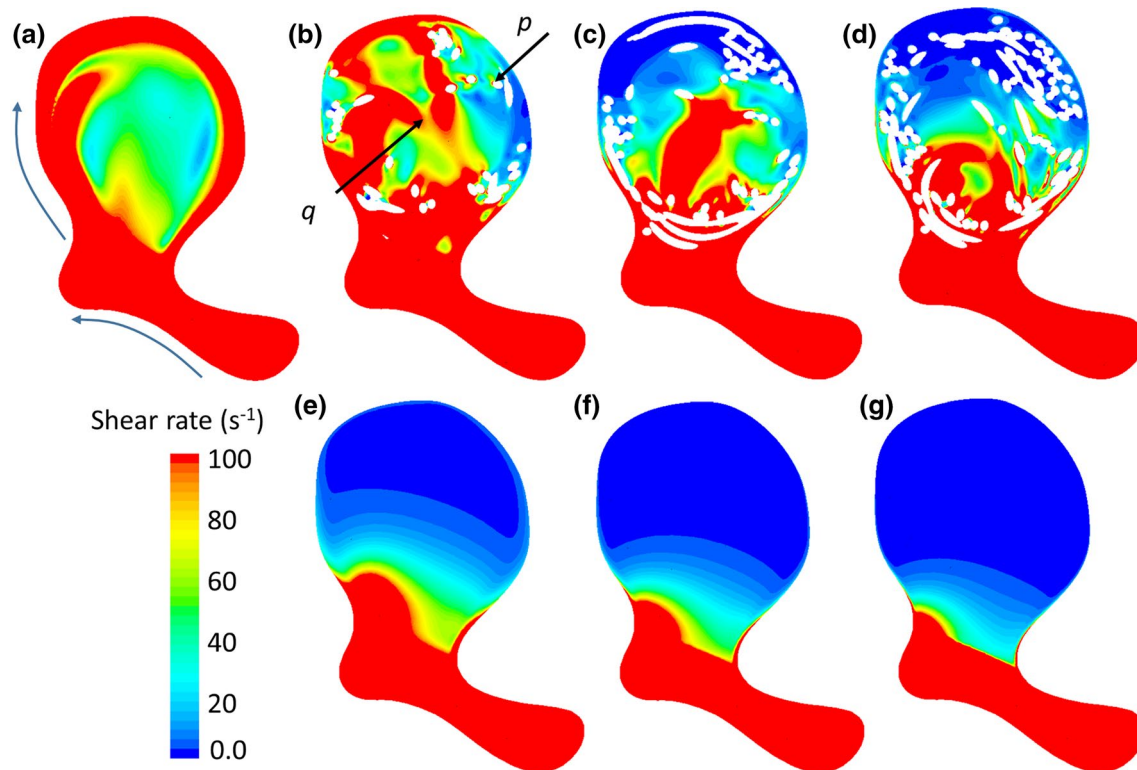


**Fig. 7** Shear rate of the blood flow in the cross-sectional plane of the aneurysm before coil embolization (a). Blue arrows show the flow direction. The results of the CD model at the packing density of 9, 18 and 27 % are illustrated in b–d, respectively. Arrows  $p$  and  $q$  show

the inner and middle regions of the aneurysm, respectively. The bottom panels show the results of the PM model at the packing density 10 % (e), 20 % (f) and 30 % (g)

$$\dot{\gamma} = 2\sqrt{II_{\mathbf{D}}}, \quad (21)$$

where  $II_{\mathbf{D}}$  is the second invariant of the strain rate tensor  $\mathbf{D}$ , given by

$$\mathbf{D} = \frac{1}{2}(\nabla\mathbf{u} + \nabla\mathbf{u}^T), \quad (22)$$

Figure 7 shows the shear rate in the cross-sectional plane of the aneurysm. Prior to coil embolization, a shear rate higher than  $100 \text{ s}^{-1}$  was found around the aneurysm wall because of the swirling flow. In the results of the CD model, the shear rate around the aneurysm wall was locally diminished, particularly in the inner region (shown by arrow  $p$  in Fig. 7b), whereas a high shear rate region formed in the middle region of the aneurysm (shown by arrow  $q$  in Fig. 7b) at a PD of 9 %. With increasing PD, the shear rate dramatically decreased in the inner region of the aneurysm to lower than  $10 \text{ s}^{-1}$ ; however, it locally increased around the coil surfaces from the neck to the middle region at a PD of 18 %. This tendency was also shown at a PD of 27 %. The results of the PM model show different tendencies compared with the results of the CD model. At a low PD of 10 %, the shear rate gradually decreased from the neck to the center region, and thus, the shear rate in the inner

region was lower than  $10 \text{ s}^{-1}$ . The value of the shear rate in the neck region decayed with increasing PD.

For quantitative evaluations of the flow stagnation based on the coil embolization, we focused on changes of momentum and kinetic energy of the flow in the aneurysm by introducing the flow momentum ratio (FMR) [25] and flow kinetic energy ratio (FER) as

$$\text{FMR} [\%] = 100 \frac{\int_V \rho |\mathbf{u}| dV}{\int_V \rho |\mathbf{u}_0| dV} \quad (23)$$

$$\text{FER} [\%] = 100 \frac{\frac{1}{2} \int_V \rho \mathbf{u} \cdot \mathbf{u} dV}{\frac{1}{2} \int_V \rho \mathbf{u}_0 \cdot \mathbf{u}_0 dV}, \quad (24)$$

where  $V$  is the coil-embolized region of the aneurysm,  $\mathbf{u}_0$  and  $\mathbf{u}$  are the velocity vector before and after coil embolization, respectively. In the analysis by the PM model, the coil-embolized region used to evaluate FMR and FER is identical to the aneurysm region shown in Fig. 1d. However, in the analysis by the CD model, the coil-embolized region is not determined in the same way; its boundary in the aneurysm is not explicitly represented because of the inhomogeneous coil distribution in the neck region. Thus,





**Fig. 8** Coil-embolized aneurysm region defined in pink used in the evaluations for FMR (Eq. 23), FER (Eq. 24) and FSR (Eq. 25)

the coil-embolized region is manually determined as shown in Fig. 8.

Figure 9 shows the FMR and FER against the PDs obtained by the flow analyses with the CD model and the PM model. The blue region in each figure illustrates the range obtained by the CFD studies using various idealized geometries of the aneurysm with the PM model [25]. In the CD model, the FMR gradually decayed with increasing PD and reached 15 % at PD ≈ 27 %. The range between maximum and minimum values based on the difference of the coil configuration also gradually decreased and finally reached approximately 7 % at PD ≈ 27 %. Minimum values were in the range based on the idealized geometry, whereas maximum values exceeded this range for all PDs. Conversely, the PM model gave FMRs in the range based on the idealized geometry for all PDs. The FMR in the PM model dramatically decayed with increasing PD, and its values were always lower than those of the FMR in all CD model cases regardless of PD. Similar to the FMR, the FERs decreased as PD increased, the rates of decrease were different between the CD model and PM model, and the variations attributed to the coil configuration became small in the CD model with the increase in PD.

To evaluate the change in the shear flow field in the aneurysm, the flow shear rate ratio (FSR) is defined as

$$FSR [\%] = 100 \frac{\int_V \rho \dot{\gamma} dV}{\int_V \rho \dot{\gamma}_0 dV}, \tag{25}$$

where  $\dot{\gamma}_0$  and  $\dot{\gamma}$  are the shear rate before and after coil embolization, respectively.

Figure 10 shows the FSR against the PDs obtained by flow analyses using the CD model and the PM model. The FSR of the CD model mildly decreased with increasing PD

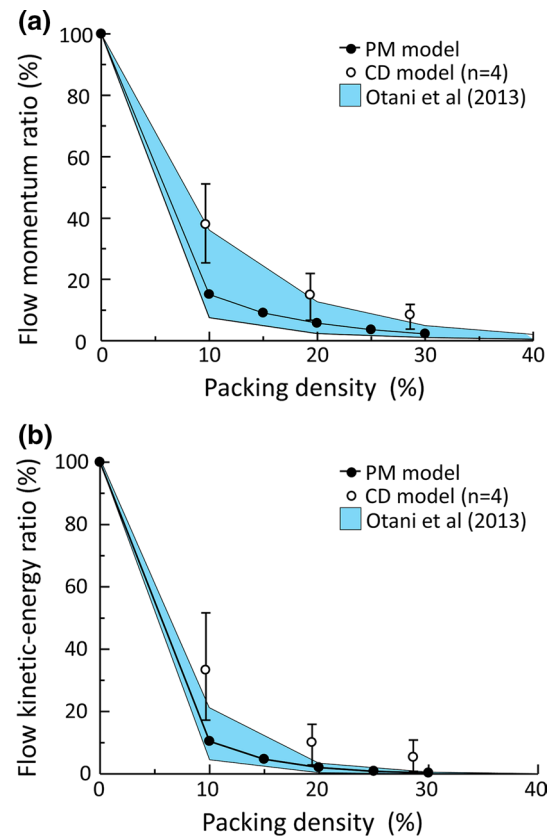


**Fig. 9** Flow momentum ratio (FMR) (a) and flow kinetic energy ratio (FER) (b) against the packing density. Filled and open circles show the results of the PM model and CD model, respectively. Error bars of the results of the CD model show the maximum and minimum values based on the differences in the coil configuration obtained by changing the deployment position and angle ( $n = 4$ ). The blue regions show the range of the CFD results in various idealized geometries of the aneurysm in the study [25]

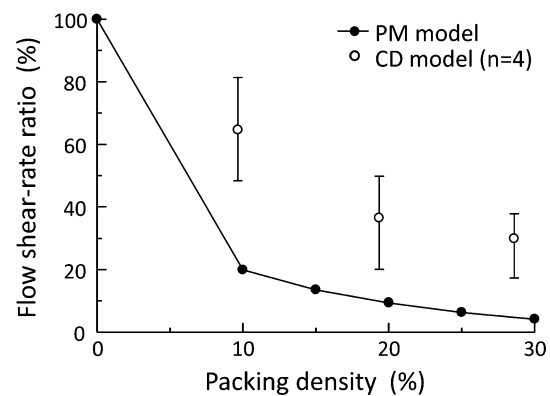


**Fig. 10** Flow shear rate ratio (FSR) against the packing density. Black and open circles show the results of the PM and CD models, respectively. Error bars of the results of the CD model show the maximum and minimum values based on the differences in the coil configuration obtained by changing the deployment position and angle ( $n = 4$ )

in all coil configurations. Its average and the range of the minimum and maximum remained at approximately 30 and 20 % even at the high PD  $\approx 27$  %. In contrast, the FSR of the PM model dramatically decayed with increasing PD and reached approximately 4 % at PD = 30 %.

## 4 Discussion

### 4.1 Effects of coil configuration on the flow characteristics

In the present study, CFD studies of the blood flow in an aneurysm with realistic coil configurations were carried out using the CD model. We discuss the validity of the coil configuration in the CD model. Morales et al. [24] measured 2D coil distributions in aneurysms in rabbits by observing histological slices. They reported that the coil tends to be located near the aneurysm periphery for PD < 20 %, whereas the radial distribution becomes more homogeneous for PD  $\cong 30$  %. These tendencies are in good agreement with the results of the CD model (Fig. 5) and suggest the validity of the constructed coil configuration in the CD model.

An increase in PD progressed the flow stagnation in the aneurysm, which was found in the results using both CD and PM models, as shown in Figs. 6 and 9. These global flow characteristics with increasing PD showed good agreement with the results of existing CFD studies [1, 21]. Moreover, the effects of the coil configuration on the global flow stagnation were also consistent with Morales et al. [21], which found that variations in the spatiotemporally averaged velocities gradually decreased with increasing PD and that the effects of differences in coil configuration were sufficiently small at a PD of approximately 30 % [21]. Therefore, we believe that the global flow characteristics in the coil-embolized aneurysms shown in this study are consistent with those from existing studies, although a quantitative comparison between our CFD results and existing studies is difficult because of the differences in aneurysm geometries and boundary conditions.

For further evaluations of the flow characteristics of the coil-embolized aneurysm, we focused on the shear rate defined in Eq. (18). As shown in Figs. 7 and 10, the shear rate dramatically decreased in the inner region (shown by the arrow  $p$  in Fig. 7b) because of the coil embolization, while it locally increased around the coil surfaces in the entrance neck region regardless of PD, which was not observed in the results using the PM model. The FSR and its variation based on the difference of the coil configuration mildly decreased with increasing PD. This result indicates that the presence of the coil enhances the strong shear flow and that the characteristics of the shear flow depend

on the coil configuration even at a PD adequate for clinical practice [31, 32]. In the present case, the shear flow is induced by the no-slip velocity on the coil surfaces in the neck region, while its strength gradually decreases with the increasing degree of flow stagnation in the aneurysm based on the coil embolization. These characteristics are influenced by the specific configuration of the coils, which therefore produce the variations in the FSR.

Generally, sparse packing in the entrance neck region (clinically called the neck remnant) increases the risk of inducing aneurysm recurrence [13, 29, 35, 36]. As mentioned above, the coil configuration is closely related to the strength of the shear flow in the neck region. It is commonly known that the strength of the shear rate plays an essential role in blood clot formation [4, 10, 33, 37]; e.g., Tipple and Müller-Mohnssen [33] observed blood clot formation in the low shear rate region ( $<15 \text{ s}^{-1}$ ). According to our findings, we speculate that the strong shear flow induced by insufficient coil embolization in the neck region of the aneurysm may prevent the blood clot formation required to keep the treatment effective.

## 5 Utility and limitations of the PM model

The present results also demonstrate the utility and limitations of the PM model through comparing the results of the CD and PM models. As shown in Fig. 9, FMRs and FERs in both models decreased with increasing PD, whereas the maximum values of both FMRs and FERs exceeded the ranges defined by the idealized geometry with the PM model in the previous study [25] regardless of PD. In the PM model, the effects of coil embolization are explained by the assumption that the coil-embolized region, including the neck region, has identical PD. However, in the CD model, the coil distribution, especially in the neck region, is locally sparse and inhomogeneous; thus, relatively high blood velocity remains in the neck region, which may cause FMR and FER to exceed the range obtained in the previous study [25].

The difference between the CD model and PM model is more clearly shown in the results of the distribution and value of the shear rate. The shear rate distribution and the FSR showed different tendencies between both models, as shown in Figs. 7 and 10. The strong shear flow found in the results of the CD model was not found in that of the PM model, and moreover, the FSR in the results of the PM model dramatically decayed with increasing PD. Given that the presence of the coil is implicitly represented in the PM model, it is difficult to represent the shear flow formation that is mainly induced by the no-slip velocity of the coil surface.

From the medical/clinical application viewpoint, blood flow analysis with the PM model is an attractive approach

to evaluate the degree of flow stagnation after coil embolization, without paying heed to the geometric complexity of coil configuration. However, our results show that a model explicitly incorporating the coil configuration, as in the present blood flow analysis with the CD model, is necessary for the fundamental understanding of the effects of coil embolization on the blood flow characteristics, resulting in further predictions of treatment effectiveness.

## 6 Further considerations

There are three areas in the present approach that can be discussed and improved upon. First, the CD model is currently limited in its ability to express the physically consistent behavior of actual coils. The physical parameters of the coil that expressed the dynamics of the coils were set empirically; moreover, only two elastic resistances, stretching and bending, were taken into account. The coil configuration was determined by three independently defined resistances, i.e., the stretching, bending and torsional resistances. To express the coil dynamics accurately, the torsional resistance needs to be considered. In future work, a more physically accurate coil model is required for the detailed evaluation of the variation of the coil configuration available in the aneurysm. Furthermore, the adequate setting of the reference state of the coil is also an important point. The reference state of the coil was set to be straight in the present simulation, and thus the coil was distributed around the aneurysm surface to maximize its curvature in the coil deployment simulation. In clinical practice, coils with a two-dimensional helical or a 3-D loop structure are generally used for efficient coil deployment [38]. In the procedure of coil embolization, the first coil is selected such that its loop size is near to that of the diameter of the aneurysm, and subsequent coils with relatively small loop sizes compared with existing coils are deployed in the aneurysm to increase the PD and the homogeneity of the coil distribution. The consideration of the reference state of the coils is also required to obtain a more realistic coil distribution. Eventually, the difficulty of the experimental validation of the computational model of the coil embolization makes these further improvements highly challenging. 3-D measurement of the coil configuration *in vivo* is limited because of the spatial resolution of current medical imaging. Furthermore, coils are manually deployed using a trial-and-error process in clinical practice, and thus the final coil configuration in the aneurysm seems to be different in each situation. To address these issues, both the development of a 3-D *in vitro* measurement technique and a large coil configuration dataset would be required. Second, the pulsatility of blood flow was not considered in the blood

flow analyses. Geers et al. [14] reported that the steady flow assumption can approximate the temporal average of the unsteady flow for the blood flow analysis in a cerebral aneurysm. We also examined the effects of flow pulsatility on the CFD results by imposing a pulsatile flow at the inlet of the coil-embolized aneurysm with a PD of 9 and 27 %. Here, the time course of flow rate in one cardiac cycle was determined by the measurement results from Ford et al. [11]. Temporally averaged solutions showed good agreement with those in the steady flow condition, and these differences were remarkably small compared with the temporal variations because of the pulsatility, approximately 2 and 6 % for flow momentum and 3 and 7 % for shear rate at both the PDs, respectively. Thus, we concluded that the steady flow simulation in this study also satisfactorily approximated the temporally averaged flow characteristics of the pulsatile flow simulation in cerebral aneurysms. However, the temporal oscillation of blood flow based on the pulsatility might not be negligible around the coils, where vortex shedding may appear by entering the blood flow directly in the aneurysm and causing a disturbance around the coils. In terms of the biological aspect, this temporal oscillation (e.g., expressed by the wall shear stress) induces a biological reaction in the endothelial cells such that they remodel the arterial tissues [8]. A more detailed evaluation of the effects of coil embolization with the CD model will enable the prediction of this biological reaction based on the specific flow characteristics caused by coil embolization. Third, sensitivity analyses of the coil configurations, patient-specific aneurysm geometry and hemodynamics are limited in this study. Although we believe that the shear flow generally appears in the neck region because of the existence of the embolization coils, its strength and spatial distribution are influenced by numerous factors. To evaluate what and to what extent is the quantitative effect of the coil embolization on the blood flow characteristics, numerical experiments using large patient samples and variations of the coil configuration should be conducted as a next step. Fourth, the experimental validation of the detailed flow characteristics in the coil-embolized aneurysm is still challenging because of the lack of medical imaging techniques to capture the microflow field in complex-tangled coils in the aneurysm. Meanwhile, the *in vivo* experimental measurement of the microblood flow in the brain is expected in many fields such as neurobiology and tumor research, and attractive measurement techniques have been subsequently developed, e.g., [18]. These techniques may be capable of measuring the microblood flow fields in coils, which has huge potential for not only the experimental validation of our CFD study but also the improvement of the computational modeling of the effects of coil embolization on the blood flow in the aneurysm.

## 7 Conclusions

In the present study, we investigated the effects of coil configuration on blood flow characteristics in coil embolization for a patient-specific cerebral aneurysm. The coil configurations deployed in the aneurysm were obtained using coil deployment simulation, and blood flow simulation was carried out. The increase in PD increased the homogeneity of the coil distribution in the aneurysm. The increase of these factors enhanced the overall flow stagnation and diminished the effects of the coil configuration attributed to the difference of the coil deployment condition, which was illustrated by the reduction of the total momentum magnitude and kinetic energy. However, the shear rate around the coils in the entrance neck region was relatively high, and its total reduction ratio in the aneurysm showed a large variation based on differences in coil configuration even at the high PD (> 25 %). These local effects of coil configuration were obviously not represented by the homogeneous PM model of the blood flow in the coil-embolized aneurysm. Because the sufficient shear rate reduction is a key factor in inducing the blood clot formation associated with the treatment effectiveness, the present case study exhibited an interesting speculation in that the coil configuration affects the local shear flow field in the aneurysm even at a clinically adequate PD. Further considerations using large sample data, variations of the coil configuration and PD would be beneficial for understanding to what extent the embolized coils disturb the local flow characteristics and promote blood clot formation in the aneurysm.

**Acknowledgments** This work was supported in part by the Japan Society for the Promotion of Science (JSPS) Grants-in-Aid for Scientific Research (No. 23650261), JSPS Research Fellowships for Young Scientist (No. 14J01622) and MEXT as a Priority Issue (Integrated computational life science to support personalized and preventive medicine) to be tackled by using post-K computer.

**Compliance with ethical standards**

**Conflict of interest** None.

## References

- Babiker MH, Chong B, Gonzalez LF, Cheema S, Frakes DH (2013) Finite element modeling of embolic coil deployment: multifactor characterization of treatment effects on cerebral aneurysm hemodynamics. *J Biomech* 46:2809–2816. doi:10.1016/j.jbiomech.2013.08.021
- Baráth K, Cassot F, Rüfenacht DA, Fasel JH (2004) Anatomically shaped internal carotid artery aneurysm in vitro model for flow analysis to evaluate stent effect. *AJNR Am J Neuroradiol* 25(10):1750–1759
- Byun HS, Rhee K (2004) CFD modeling of blood flow following coil embolization of aneurysms. *Med Eng Phys* 26(9):755–761. doi:10.1016/j.medengphy.2004.06.008
- Cabel M, Meiselman HJ, Popel AS, Johnson PC (1997) Contribution of red blood cell aggregation to venous vascular resistance in skeletal muscle. *Am J Physiol* 272(2 Pt 2):H1020–H1032
- Cebral JR, Löhner R (2005) Efficient simulation of blood flow past complex endovascular devices using an adaptive embedding technique. *IEEE Trans Med Imaging* 24(4):468–476. doi:10.1109/TMI.2005.844172
- Cha KS, Balaras E, Lieber BB, Sadasivan C, Wakhloo AK (2007) Modeling the interaction of coils with the local blood flow after coil embolization of intracranial aneurysms. *J Biomech Eng* 129(6):873–879. doi:10.1115/1.2800773
- Chalouhi N, Jabbour P, Singhal S, Drueding R, Starke RM, Dalyai RT, Tjoumakaris S, Gonzalez LF, Dumont AS, Rosenwasser R, Randazzo CG (2013) Stent-assisted coiling of intracranial aneurysms: predictors of complications, recanalization and outcome in 508 cases. *Stroke* 44(5):1348–1353. doi:10.1161/STROKEAHA.111.000641
- Chatzizisis YS, Coskun AU, Jonas M, Edelman ER, Feldman CL, Stone PH (2007) Role of endothelial shear stress in the natural history of coronary atherosclerosis and vascular remodeling: molecular, cellular, and vascular behavior. *J Am Coll Cardiol* 49(25):2379–2393. doi:10.1016/j.jacc.2007.02.059
- Ergun S (1952) Fluid flow through packed columns. *Chem Eng Prog* 48:89–94
- Flamm MH, Diamond SL (2012) Multiscale systems biology and physics of thrombosis under flow. *Ann Biomed Eng* 40(11):2355–2364. doi:10.1007/s10439-012-0557-9
- Ford MD, Alperin N, Lee SH, Holdsworth DW, Steinman DA (2005) Characterization of volumetric flow rate waveforms in the normal internal carotid and vertebral arteries. *Physiol Meas* 26(4):477–488. doi:10.1088/0967-3334/26/4/013
- Groden C, Laudan J, Gatchell S, Zeumer H (2001) Three-dimensional pulsatile flow simulation before and after endovascular coil embolization of a terminal cerebral aneurysm. *J Cereb Blood Flow Metab* 21(12):1464–1471. doi:10.1097/00004647-200112000-00011
- Gallas S, Pasco A, Cottier JP, Gabrillargues J, Drouineau J, Cognard C, Herbreteau D (2005) A multicenter study of 705 ruptured intracranial aneurysms treated with Guglielmi detachable coils. *AJNR Am J Neuroradiol* 26(7):1723–1731
- Geers AJ, Larrabide I, Morales HG, Frangi AF (2014) Approximating hemodynamics of cerebral aneurysms with steady flow simulations. *J Biomech* 47(1):178–185. doi:10.1016/j.jbiomech.2013.09.033
- Jeong W, Han MH, Rhee K (2013) Effects of framing coil shape, orientation, and thickness on intra-aneurysmal flow. *Med Biol Eng Comput* 51(9):981–990. doi:10.1007/s11517-013-1073-2
- Kakalis NM, Mitsos AP, Byrne JV, Ventikos Y (2008) The haemodynamics of endovascular aneurysm treatment: a computational modelling approach for estimating the influence of multiple coil deployment. *IEEE Trans Med Imaging* 27(6):814–824. doi:10.1109/TMI.2008.915549
- Khanafar K, Berguer R, Schlicht M, Bull J (2009) Numerical modeling of coil compaction in the treatment of cerebral aneurysms using porous media theory. *J Porous Media* 12:887–897. doi:10.1615/JPorMedia.v12.i9.50
- Landolt A, Obrist D, Wyss MT, Barrett M, Langer D, Jolivet R, Soltysinski T, Roesgen T, Weber B (2013) Two-photon microscopy with double-circle trajectories for in vivo cerebral blood flow measurements. *Exp Fluids* 54:1523. doi:10.1007/s00348-013-1523-5
- Mishra B, Rajamani R (1992) The discrete element method for the simulation of ball mills. *Appl Math Model* 16(11):598–604. doi:10.1016/0307-904X(92)90035-2
- Mitsos AP, Kakalis NM, Ventikos YP, Byrne JV (2008) Haemodynamic simulation of aneurysm coiling in an anatomically accurate computational fluid dynamics model: technical note. *Neuroradiology* 50(4):341–347. doi:10.1007/s00234-007-0334-x



21. Morales HG, Kim M, Vivas EE, Villa-Uriol MC, Larrabide I, Sola T, Guimaraens L, Frangi AF (2011) How do coil configuration and packing density influence intra-aneurysmal hemodynamics? *AJNR Am J Neuroradiol* 32(10):1935–1941. doi:[10.3174/ajnr.A2635](https://doi.org/10.3174/ajnr.A2635)
22. Morales HG, Larrabide I, Geers AJ, San Roman L, Blasco J, Macho JM, Frangi AF (2013) A virtual coiling technique for image-based aneurysm models by dynamic path planning. *IEEE Trans Med Imaging* 32(1):119–129. doi:[10.1109/TMI.2012.2219626](https://doi.org/10.1109/TMI.2012.2219626)
23. Morales HG, Larrabide I, Geers AJ, Aguilar ML, Frangi AF (2013) Newtonian and non-Newtonian blood flow in coiled cerebral aneurysms. *J Biomech* 46(13):2158–2164. doi:[10.1016/j.jbiomech.2013.06.034](https://doi.org/10.1016/j.jbiomech.2013.06.034)
24. Morales HG, Larrabide I, Geers AJ, Dai D, Kallmes DF, Frangi AF (2013) Analysis and quantification of endovascular coil distribution inside saccular aneurysms using histological images. *J Neurointerv Surg* 5(Suppl 3):iii33–iii37. doi:[10.1136/neurintsurg-2012-010456](https://doi.org/10.1136/neurintsurg-2012-010456)
25. Otani T, Nakamura M, Fujinaka T, Hirata M, Kuroda J, Shibano K, Wada S (2013) Computational fluid dynamics of blood flow in coil-embolized aneurysms: effect of packing density on flow stagnation in an idealized geometry. *Med Biol Eng Comput* 51(8):901–910. doi:[10.1007/s11517-013-1062-5](https://doi.org/10.1007/s11517-013-1062-5)
26. Otani T, Ii S, Fujinaka T, Hirata M, Kuroda J, Shibano K, Wada S (2013) Development of a virtual coil model for blood flow simulation in coil-embolized aneurysms. In: *ASME Proceedings of IMECE 2013*, IMECE2013-64435-V03AT03A035. doi:[10.1115/IMECE2013-64435](https://doi.org/10.1115/IMECE2013-64435)
27. Otani T, Ii S, Fujinaka T, Hirata M, Kuroda J, Shibano K, Wada S (2014) Blood flow analysis in patient-specific cerebral aneurysm models with realistic configuration of embolized coils. *IFMBE Proc* 43:343–346. doi:[10.1007/978-3-319-02913-9\\_87](https://doi.org/10.1007/978-3-319-02913-9_87)
28. Piotin M, Spelle L, Mounayer C, Salles-Rezende MT, Giansante-Abud D, Vanzin-Santos R, Moret J (2007) Intracranial aneurysms: treatment with bare platinum coils—aneurysm packing, complex coils, and angiographic recurrence. *Radiology* 243(2):500–508. doi:[10.1148/radiol.2431060006](https://doi.org/10.1148/radiol.2431060006)
29. Piotin M, Blanc R, Spelle L, Mounayer C, Piantino R, Schmidt PJ, Moret J (2010) Stent-assisted coiling of intracranial aneurysms: clinical and angiographic results in 216 consecutive aneurysms. *Stroke* 41(1):110–115. doi:[10.1161/STROKEAHA.109.558114](https://doi.org/10.1161/STROKEAHA.109.558114)
30. Schirmer CM, Malek AM (2010) Critical influence of framing coil orientation on intra-aneurysmal and neck region hemodynamics in a sidewall aneurysm model. *Neurosurgery* 67(6):1692–1702. doi:[10.1227/NEU.0b013e3181f9a93b](https://doi.org/10.1227/NEU.0b013e3181f9a93b)
31. Sluzewski M, van Rooij WJ, Slob MJ, Bescós JO, Slump CH, Wijnalda D (2004) Relation between aneurysm volume, packing, and compaction in 145 cerebral aneurysms treated with coils. *Radiology* 231(3):653–658. doi:[10.1148/radiol.2313030460](https://doi.org/10.1148/radiol.2313030460)
32. Tamatani S, Ito Y, Abe H, Koike T, Takeuchi S, Tanaka R (2002) Evaluation of the stability of aneurysms after embolization using detachable coils: correlation between stability of aneurysms and embolized volume of aneurysms. *AJNR Am J Neuroradiol* 23(5):762–767
33. Tippe A, Müller-Mohnssen H (1993) Shear dependence of the fibrin coagulation kinetics in vitro. *Thromb Res* 72:379–388
34. Unverdi SO, Tryggvason G (1992) A front-tracking method for viscous, incompressible, multi-fluid flows. *J Comput Phys* 100:25–37
35. Raymond J, Guilbert F, Weill A, Georganos SA, Juravsky L, Lambert A, Lamoureux J, Chagnon M, Roy D (2003) Long-term angiographic recurrences after selective endovascular treatment of aneurysms with detachable coils. *Stroke* 34(6):1398–1403. doi:[10.1161/01.STR.0000073841.88563.E9](https://doi.org/10.1161/01.STR.0000073841.88563.E9)
36. Roy D, Milot G, Raymond J (2001) Endovascular Treatment of Unruptured Aneurysms. *Stroke* 32(9):1998–2004. doi:[10.1161/hs0901.095600](https://doi.org/10.1161/hs0901.095600)
37. Weiss HJ, Turitto VT (1986) Role of shear rate and platelets in promoting fibrin formation on rabbit subendothelium. Studies utilizing patients with quantitative and qualitative platelet defects. *J Clin Invest* 78:1072–1082
38. White JB, Ken CG, Cloft HJ, Kallmes DF (2008) Coils in a nutshell: a review of coil physical properties. *AJNR Am J Neuroradiol* 29(7):1242–1246. doi:[10.3174/ajnr.A1067](https://doi.org/10.3174/ajnr.A1067)



**Tomohiro Otani, Ph.D.** completed his Master's degree and Ph.D. degree at Osaka University in 2013 and 2016, respectively. He is currently an Assistant Professor at Osaka University.



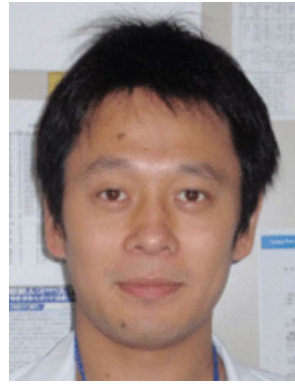
**Satoshi Ii, Ph.D.** completed his Master's degree and Ph.D. degree at Tokyo Institute of Technology in 2006 and 2008, respectively. He is now a Research Associate Professor at Osaka University. He engages computational mechanics and biomechanics.



**Tomoyoshi Shigematsu, M.D., Ph.D.** graduated from Faculty of Osaka University Medical School in 2004 and received his Ph.D. degree at Osaka University in 2015. He is a board-certified Neurosurgeon and Neurointerventionalist. He is currently research fellow at Mount Sinai St. Luke's and Mount Sinai Roosevelt, NY.



**Toshiyuki Fujinaka, M.D., Ph.D.** graduated from Faculty of Osaka University Medical School in 1992. He is a board-certified Neurosurgeon and Neurointerventionalist. He is currently director of Neurosurgery in National Hospital Organization Osaka National Hospital.



**Tomohiko Ozaki, M.D., Ph.D.** received his degree of medical doctor in Osaka University School of Medicine in 2005. After graduate, he worked at the Department of Neurosurgery in Osaka National Hospital and the Department of Neurosurgery in Kansai Rosai Hospital. He is currently working at the Department of Neurosurgery in Osaka University Hospital. He is a board-certified member of Japanese Society of Neurosurgery and board-certified member of Japanese Society for Neuroendovascular Therapy.



**Masayuki Hirata, B.S., M.S. and M.D. and Ph.D.** graduated from Faculty of Engineering, The University of Tokyo in 1985 and Osaka University Medical School in 1994. He is a board-certified neurosurgeon specialized in functional neurosurgery and epilepsy surgery. He is developing brain–machine interfaces using intracranial electrodes. He is also a board-certified endovascular neurosurgeon. He is currently a Specially Appointed Associate Professor, Department of Neurosurgery,

Osaka University Medical School serving as a leader of neural engineering group.



**Shigeo Wada, Ph.D.** received Ph.D. from Osaka University in 1991 and is currently a Professor of Mechanical Science and Bioengineering in Osaka University his expertise is computational biomechanics on the respiratory and cardiovascular systems. He is a member of World Council of Biomechanics.